





# Steady Rayleigh-Bénard convection between no-slip boundaries

Baole Wen<sup>1</sup>,†, David Goluskin<sup>2</sup>,† and Charles R. Doering<sup>1,3,4</sup>

(Received 14 October 2021; revised 22 October 2021; accepted 21 November 2021)

The central open question about Rayleigh–Bénard convection – buoyancy-driven flow in a fluid layer heated from below and cooled from above – is how vertical heat flux depends on the imposed temperature gradient in the strongly nonlinear regime where the flows are typically turbulent. The quantitative challenge is to determine how the Nusselt number Nudepends on the Rayleigh number Ra in the  $Ra \to \infty$  limit for fluids of fixed finite Prandtl number Pr in fixed spatial domains. Laboratory experiments, numerical simulations and analysis of Rayleigh's mathematical model have yet to rule out either of the proposed 'classical'  $Nu \sim Ra^{1/3}$  or 'ultimate'  $Nu \sim Ra^{1/2}$  asymptotic scaling theories. Among the many solutions of the equations of motion at high Ra are steady convection rolls that are dynamically unstable but share features of the turbulent attractor. We have computed these steady solutions for Ra up to  $10^{14}$  with Pr = 1 and various horizontal periods. By choosing the horizontal period of these rolls at each Ra to maximize Nu, we find that steady convection rolls achieve classical asymptotic scaling. Moreover, they transport more heat than turbulent convection in experiments or simulations at comparable parameters. If heat transport in turbulent convection continues to be dominated by heat transport in steady rolls as  $Ra \to \infty$ , it cannot achieve the ultimate scaling.

**Key words:** Bénard convection

#### 1. Introduction

Rayleigh–Bénard convection (RBC) is the buoyancy-driven flow in a fluid layer heated from below and cooled from above in the presence of gravity. The emergent convective flow enhances heat flux from the warm bottom boundary to the cool top boundary beyond the conductive flux from diffusion alone. This dimensionless enhancement factor – the

† Email addresses for correspondence: baolew@umich.edu, goluskin@uvic.ca

<sup>&</sup>lt;sup>1</sup>Department of Mathematics, University of Michigan, Ann Arbor, MI 48109-1043, USA

<sup>&</sup>lt;sup>2</sup>Department of Mathematics & Statistics, University of Victoria, Victoria, BC, V8P 5C2, Canada

<sup>&</sup>lt;sup>3</sup>Department of Physics, University of Michigan, Ann Arbor, MI 48109-1040, USA

<sup>&</sup>lt;sup>4</sup>Center for the Study of Complex Systems, University of Michigan, Ann Arbor, MI 48109-1042, USA

ratio of bulk-averaged vertical heat flux from both conduction and convection to the flux from conduction alone – defines the Nusselt number Nu. In Rayleigh's mathematical model (Rayleigh 1916) Nu depends on several dimensionless quantities characterizing the problem at hand: (i) what we now call the Rayleigh number Ra, which is proportional to the imposed temperature drop across the layer, (ii) the fluid's Prandtl number Pr, which is the ratio of kinematic viscosity to thermal diffusivity and (iii) details of the spatial domain, often captured by an aspect ratio  $\Gamma$  that is a ratio of a horizontal length scale to the vertical layer height.

Convection is coherent at Ra values not too far above the critical value  $Ra_c$  beyond which the conductive no-flow state is linearly unstable. By coherent we mean flows with few scales present; spatial scales might include a horizontal period and the vertical thickness of boundary layers, and temporally the flow may be steady or time-periodic. Meanwhile, convection is turbulent at the large Ra values pertinent to many engineering and scientific applications. Turbulent flows are complex and contain a range of spatial and temporal scales and, in the present context, have thermal and viscous boundary layers at the top and bottom boundaries from which thermal plumes emerge and mix the bulk. In a given domain it is expected that a scaling of Nu with respect to both Pr and Ra will emerge in the  $Ra \to \infty$  limit (Kadanoff 2001).

After nearly a century of increasingly sophisticated mathematical analysis, increasingly resolved direct numerical simulations (DNS) and increasingly refined laboratory experiments, two quantitatively distinct conjectures remain in contention for the heat transport scaling law at large Ra (Chillà & Schumacher 2012; Doering 2020). The two conjectures follow from heuristic physical arguments that both seem plausible but give incompatible predictions: the 'classical' scaling  $Nu \sim Pr^0Ra^{1/3}$  and the 'ultimate' scaling  $Nu \sim Pr^{1/2}Ra^{1/2}$ , with the latter sometimes including logarithmic-in-Ra modifications.

For RBC between flat, no-slip, isothermal boundaries, rigorous analysis of the governing equations has yielded upper bounds of the form  $Nu \leq O(Ra^{1/2})$  uniformly in Pr and  $\Gamma$ (Howard 1963; Doering & Constantin 1996), but this still allows for either classical or ultimate scaling. Upper bounds that rule out ultimate scaling by being asymptotically smaller than  $O(Ra^{1/2})$  have been derived in the limit of infinite Pr (Doering, Otto & Reznikoff 2006; Otto & Seis 2011; Whitehead & Doering 2012) and for two-dimensional convection between stress-free boundaries (Whitehead & Doering 2011). For the no-slip boundaries relevant to experiments, however, it remains an open question whether an upper bound asymptotically smaller than  $Ra^{1/2}$  is possible.

In view of the problem's stubbornness, a new strategy is called for to determine – or at least to bound – Nu as a function of Ra, Pr and  $\Gamma$ . Towards that end we have undertaken an indirect approach consisting of two parts. The first part is to study coherent flows for which one can reasonably hope to determine asymptotic heat transport, and the second part is to investigate how transport by those coherent flows compares with transport by turbulent convection. The simplest coherent flows are steady – i.e. time-independent – solutions of the equations of motion. Many such states exist, although they are generally unstable at large Ra. We focus on what might be called the simplest type of steady states: two-dimensional convection rolls like the counter-rotating pairs shown in figure 1(a,b). In horizontally periodic or infinite domains in two or three dimensions, such rolls bifurcate supercritically from the conductive state in the linear instability identified by Rayleigh (1916). A roll pair of any width-to-height aspect ratio  $\Gamma$  admitted by the domain exists for sufficiently large Ra.

For steady rolls, the dependence of Nu on the parameters  $(\Gamma, Pr, Ra)$  at asymptotically large Ra is accessible to computation. As for whether heat transport by steady rolls can be 933 R4-2

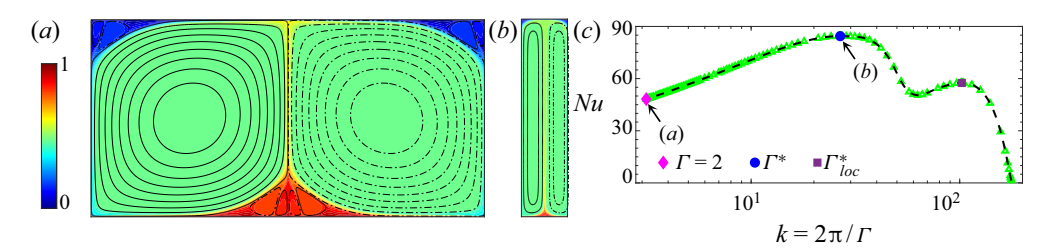


Figure 1. Steady convection rolls at  $Ra = 10^9$  and Pr = 1 with (a)  $\Gamma = 2$  and (b) the value  $\Gamma^* \approx 0.235$ that maximizes Nu at these values of Ra and Pr. Colour indicates temperature, and streamlines are shown for anticlockwise (solid) and clockwise (dash-dotted) motions. (c) Dependence of Nu on the horizontal wavenumber  $k = 2\pi/\Gamma$  found by computing steady rolls of various aspect ratios ( $\triangle$ , green). Highlighted points are the two  $\Gamma$  shown in (a,b) along with the value  $\Gamma_{loc}^* \approx 0.0614$  that locally maximizes  $Nu(\Gamma)$ . Cubic spline interpolation (dashed line) is used to find  $\Gamma^*$  and  $\Gamma_{loc}^*$  precisely.

connected to transport by turbulence, there are several reasons for optimism. Relationships between turbulent attractors and the unstable coherent states embedded therein have been established in models of wall-bounded shear flows (Graham & Floryan 2021), where particular steady states, travelling waves and time-periodic states have been found that closely reflect turbulent flows in terms of integral quantities as well as particular flow structures. Analogous study of RBC began only recently but indeed suggests that certain steady states capture qualitative aspects of turbulent convection (Sondak, Smith & Waleffe 2015; Waleffe, Boonkasame & Smith 2015; Kooloth, Sondak & Smith 2021; Motoki, Kawahara & Shimizu 2021). Our findings add to this evidence. The desire to understand and perhaps strengthen the mathematical bound  $Nu \leq O(Ra^{1/2})$  is further motivation for studying unstable states since bounds apply to all solutions of the governing equations regardless of stability. It is an open question whether any solutions can achieve ultimate scaling, let alone turbulent solutions.

Here we report numerical computations of steady convection rolls for a Pr = 1 fluid contained between no-slip isothermal top and bottom boundaries. We reach sufficiently large Ra values to convincingly reveal several asymptotic scalings of Nu, depending on the horizontal periods of the rolls. These are the first clearly asymptotic scalings found for any type of flow - steady, turbulent or otherwise - for RBC in the no-slip case. Notably, the largest heat transport among steady rolls of all horizontal periods displays the classical  $Nu \sim Ra^{1/3}$  scaling. We further observe that Nu for these steady rolls is larger than turbulent Nu from all laboratory experiments and two- or three-dimensional (2-D or 3-D) simulations at comparable parameters. This observation supports the conjecture that steady states maximize Nu among all stable or unstable flows, as was recently verified for a truncated model of RBC (Olson et al. 2021) using methods that are not yet applicable to the full governing equations. If steady-roll transport continues to dominate turbulent transport as  $Ra \to \infty$ , then our finding of classical scaling for steady rolls would rule out ultimate scaling of turbulent convection.

The asymptotic scaling of steady rolls is already known in the case of stress-free velocity conditions at the top and bottom boundaries, which were considered for mathematical convenience in Rayleigh's original work. In that case  $Nu \sim Ra^{1/3}$  as  $Ra \to \infty$  at fixed Prand  $\Gamma$ , and the aspect ratio of the roll pair maximizing Nu at each Ra and Pr approaches  $\Gamma \approx 1.9$  (Chini & Cox 2009; Wen et al. 2020). Recent computations of steady rolls in the no-slip case for preasymptotic Ra values up to  $10^9$  revealed significant differences from the stress-free problem (Sondak et al. 2015; Waleffe et al. 2015). The dependence  $Nu(\Gamma)$  for no-slip rolls at fixed Ra and Pr can have multiple local maxima, as shown in figure 1(c),

and the aspect ratio  $\Gamma^*$  that globally maximizes  $Nu(\Gamma)$  approaches zero rather than a constant as  $Ra \to \infty$ . Steady rolls of Nu-maximizing aspect ratios  $\Gamma^*$  were reported in Sondak et al. (2015) for  $Ra \in [5 \times 10^6, 3 \times 10^8]$  at Pr = 1, yielding fits of  $\Gamma^* \sim Ra^{-0.217}$ and  $Nu(\Gamma^*) \sim Ra^{0.31}$ . This heat transport scaling is faster than with  $\Gamma$  fixed: computations in Waleffe et al. (2015) for  $Ra \in [5 \times 10^5, 5 \times 10^6]$  at Pr = 7 with  $\Gamma = 2$  fixed yield the fit  $Nu \sim Ra^{0.28}$ . These best-fit scaling exponents are, however, not asymptotic.

Steady convection rolls are dynamically unstable at large Ra and cannot be found by standard time integration, so we employed a purpose-written code that iteratively solves the time-independent equations. We computed rolls with  $\Gamma = 2$  fixed for  $Ra \lesssim 2 \times 10^{10}$ and with the parameter-dependent aspect ratios  $\Gamma^*$  and  $\Gamma^*_{loc}$  (cf. figure 1) that globally and locally maximize  $Nu(\Gamma)$ , respectively, for  $Ra \leq 10^{14}$ . These Ra values are evidently large enough to reach asymptotia: the results reported below strongly suggest that fixed- $\Gamma$  rolls asymptotically transport heat like  $Nu \sim Ra^{1/4}$  while the ever-narrowing rolls of aspect ratio  $\Gamma^*$  achieve the classical  $Nu \sim Ra^{1/3}$  scaling.

## 2. Computation of steady-convection-roll solutions

Following Rayleigh (1916), we model RBC using the Boussinesq approximation to the Navier–Stokes equations with constant kinematic viscosity  $\nu$ , thermal diffusivity  $\kappa$  and coefficient of thermal expansion  $\alpha$ . We non-dimensionalize lengths by the layer height h, temperatures by the fixed difference  $\Delta$  between the boundaries, velocities by the free-fall scale  $U_f = \sqrt{g\alpha h\Delta}$ , and time by the free-fall time  $h/U_f$ . Calling the horizontal coordinate x and the vertical coordinate z, the gravitational acceleration of magnitude g is in the  $-\hat{z}$ direction. The evolution equations governing the dimensionless velocity vector  $\mathbf{u} = (u, w)$ , temperature T and pressure p are then

$$\partial_t u + \mathbf{u} \cdot \nabla \mathbf{u} = -\nabla p + (Pr/Ra)^{1/2} \nabla^2 \mathbf{u} + T\hat{\mathbf{z}}, \tag{2.1a}$$

$$\nabla \cdot \boldsymbol{u} = 0, \tag{2.1b}$$

$$\partial_t T + \boldsymbol{u} \cdot \nabla T = (PrRa)^{-1/2} \nabla^2 T,$$
 (2.1c)

where

$$Ra = \frac{g\alpha h^3 \Delta}{\kappa \nu}$$
 and  $Pr = \frac{\nu}{\kappa}$ . (2.2*a*,*b*)

The dimensionless spatial domain is  $(x, z) \in [0, \Gamma] \times [0, 1]$ , and all variables are horizontally periodic. The top and bottom boundaries are isothermal with T=0 and T=1, respectively, while no-slip conditions require u to vanish on both boundaries. The conductive state (u, T) = (0, 1 - z) becomes unstable when Ra increases past the critical value  $Ra_c \approx 1708$  (Jeffreys 1928), at which a roll pair with horizontal period  $\Gamma \approx 2.016$ bifurcates supercritically. As  $Ra \to \infty$  the horizontal period of the narrowest marginally stable roll pair decreases as  $O(Ra^{-1/4})$ , while the horizontal period of the fastest-growing linearly unstable mode decreases more slowly as  $O(Ra^{-1/8})$ .

In terms of the dimensionless solutions to (2.1), the Nusselt number is

$$Nu = 1 + (PrRa)^{1/2} \langle wT \rangle, \tag{2.3}$$

where  $\langle \cdot \rangle$  denotes an average over the spatial domain and infinite time. For steady states no time average is needed.

To compute rolls at Ra values large enough to reach the asymptotic regime, we developed a numerical scheme by adapting the approach of Wen et al. (2020) and Wen &

Chini (2018) to the case of no-slip boundary conditions. In these numerics the temperature is represented using the deviation  $\theta$  from the conductive profile, meaning  $T = 1 - z + \theta$ , and the velocity is represented using a stream function  $\psi$ , where  $u = \partial_z \psi \hat{x} - \partial_x \psi \hat{z}$  so that the (negative) scalar vorticity is  $\omega = \partial_x w - \partial_z u = -\nabla^2 \psi$ . In terms of these variables, steady ( $\partial_t = 0$ ) solutions of (2.1) satisfy

$$\partial_z \psi \, \partial_x \omega - \partial_x \psi \, \partial_z \omega = (Pr/Ra)^{1/2} \, \nabla^2 \omega + \partial_x \theta, \tag{2.4a}$$

$$\nabla^2 \psi = -\omega, \tag{2.4b}$$

$$\partial_z \psi \, \partial_x \theta - \partial_x \psi \, \partial_z \theta = -\partial_x \psi + (PrRa)^{-1/2} \, \nabla^2 \theta \tag{2.4c}$$

with fixed-temperature and no-slip boundary conditions

$$\theta|_{z=0,1} = 0$$
,  $\psi|_{z=0,1} = 0$  and  $\partial_z \psi|_{z=0,1} = 0$ . (2.5*a*-*c*)

The equality of  $\psi$  values between each boundary restricts to solutions whose horizontal velocities average to zero over every vertical section.

To compute solutions of the time-independent equations (2.4) and (2.5a-c) by an iterative method, we do not need to impose all boundary conditions precisely on each iteration – the conditions need to hold only for the converged solution. Thus we do not impose (2.5c) exactly, instead using approximate boundary conditions on  $\omega$  for equation (2.4a). These are derived by Taylor expanding  $\psi$  about the top and bottom boundaries to find

$$\psi|_{z=1-\delta} = \psi|_{z=1} - \partial_z \psi|_{z=1} \delta + \partial_z^2 \psi\Big|_{z=1} \frac{\delta^2}{2} - \partial_z^3 \psi\Big|_{z=1} \frac{\delta^3}{6} + O(\delta^4), \tag{2.6a}$$

$$\psi|_{z=\delta} = \psi|_{z=0} + \partial_z \psi|_{z=0} \delta + \partial_z^2 \psi\Big|_{z=0} \frac{\delta^2}{2} + \partial_z^3 \psi\Big|_{z=0} \frac{\delta^3}{6} + O(\delta^4), \tag{2.6b}$$

where  $\delta > 0$  is small. Combining (2.4b) with (2.5b,c) and neglecting  $O(\delta^4)$  terms in (2.6) give the approximate boundary conditions

$$\partial_z \omega|_{z=1} - \frac{3}{\delta} \omega|_{z=1} - \frac{6}{\delta^3} \psi|_{z=1-\delta} = 0, \quad -\partial_z \omega|_{z=0} - \frac{3}{\delta} \omega|_{z=0} - \frac{6}{\delta^3} \psi|_{z=\delta} = 0.$$
(2.7*a*,*b*)

In computations we set  $\delta$  to be the distance between the boundary and the first interior mesh point.

The time-independent equations (2.4) are solved numerically subject to boundary conditions (2.5a,b) and (2.7) using a Newton-GMRES (generalized minimal residual) iterative scheme. The spatial discretization is spectral, using a Fourier series in x and a Chebyshev collocation method in z (Trefethen 2000). All of our computations had at least 20 collocation points in the viscous and thermal boundary layers. At Ra just above the linear instability, iterations starting from the unstable eigenmode converge to the steady rolls we seek. At larger Ra, already-computed steady rolls from nearby Ra and  $\Gamma$  values were used as the initial iterate. Every two to four Newton iterations, we change the boundary values of the iterate to match the  $\partial_{\tau}\psi=0$  boundary condition exactly. Prior to convergence this makes the boundary values slightly inconsistent with the governing equations, but the converged solutions satisfy the equations and the no-slip boundary conditions to high precision. Newton iterations were carried out until the Lebesgue  $L^2$ -norm of the residual of the governing steady equations had a relative magnitude less than  $10^{-10}$ . To accurately locate  $\Gamma^*$  and  $\Gamma^*_{loc}$ , rolls were computed at several nearby  $\Gamma$ ,

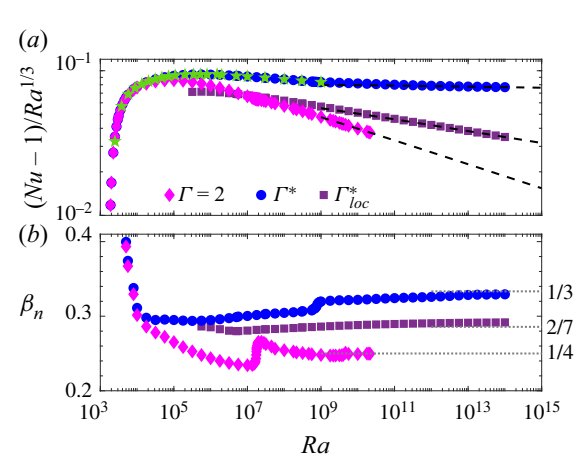


Figure 2. (a) Compensated plot of Nu-1 vs Ra for steady rolls with Pr=1 and aspect ratios of  $\Gamma=2$ ,  $\Gamma^*$  and  $\Gamma^*_{loc}$ , where the Ra-dependent values  $\Gamma^*$  and  $\Gamma^*_{loc}$  are where  $Nu(\Gamma)$  has global and local maxima, respectively (cf. figure 1). Values of Nu at  $\Gamma^*$  from Sondak et al. (2015) and Waleffe (personal communication 2020) are also shown ( $\star$ , green). Scaling fits (dashed lines) over the last decade of each data set yield exponents of 0.33, 0.29 and 0.25. (b) Finite-difference approximations of the local scaling exponent  $\beta_n = d(\log Nu)/d(\log Ra)$ . Exponents of 1/3, 2/7 and 1/4 are shown to guide the eye (grey dotted lines).

and then  $Nu(\Gamma)$  was interpolated with cubic splines like those in figure 1(c). Details of computational results, including resolutions used, are included in the supplementary material available at https://doi.org/10.1017/jfm.2021.1042.

#### 3. Results

We computed steady Pr=1 rolls for aspect ratios  $\Gamma$  encompassing the three distinguished values indicated by figure 1(c): the fixed value  $\Gamma=2$  and the Ra-dependent values  $\Gamma^*$  and  $\Gamma_{loc}^*$  that globally and locally maximize Nu over  $\Gamma$ . As previously observed by Sondak  $et\ al.\ (2015)$ , the  $Nu(\Gamma)$  curve has a single maximum when Ra is small and develops a second local maximum at smaller  $\Gamma$  when Ra increases past roughly  $2\times 10^5$ . The value of Nu at this second local maximum remains less than the value at the first, so the picture remains as in figure 1(c) with  $\Gamma^*$  on the left and  $\Gamma_{loc}^*$  on the right, in contrast to the Pr=10 and 100 cases (Sondak  $et\ al.\ 2015$ ). For most Ra values we did not compute rolls over a full sweep through  $\Gamma$  as in figure 1(c), instead searching over  $\Gamma$  only as needed to locate  $\Gamma^*$  and  $\Gamma_{loc}^*$ . The rest of this section reports Nusselt number and Reynolds number scalings for the computed steady rolls, and the supplementary material provides tabulated data.

## 3.1. Asymptotic heat transport

Figure 2 shows the dependence of Nu on Ra for steady rolls with aspect ratios  $\Gamma=2$ ,  $\Gamma^*$  and  $\Gamma_{loc}^*$ . In figure 2(a) Nu-1 is compensated by  $Ra^{1/3}$ , so the horizontal line approached by rolls of the Nu-maximizing aspect ratios  $\Gamma^*$  corresponds to classical 1/3 scaling. The downward slopes of the data for aspect ratios 2 and  $\Gamma_{loc}^*$  correspond to scaling exponents smaller than 1/3. Values of Nu at  $\Gamma^*$  computed previously for  $Ra \le 10^9$  (Sondak  $et\ al.\ 2015$ ; Waleffe, personal communication 2020) are shown in figure 2 also, and they agree with our computations very precisely – e.g. the  $Ra=10^9$  data point agrees with our value of Nu to within 0.0008 %.

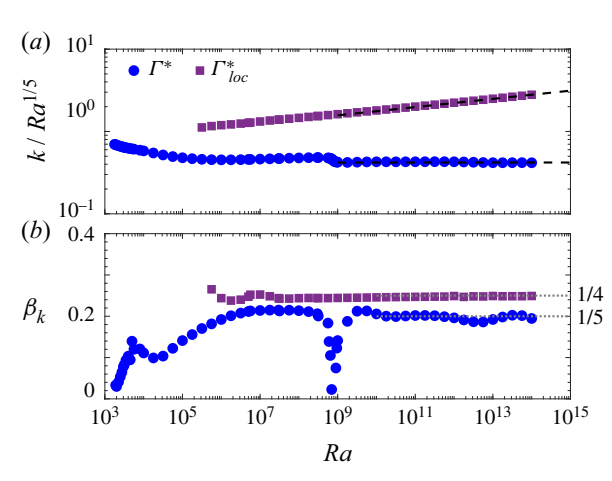


Figure 3. (a) Compensated plot of the fundamental horizontal wavenumber  $k = 2\pi/\Gamma$  vs Ra for the aspect ratios  $\Gamma^*$  and  $\Gamma^*_{loc}$  that maximize  $Nu(\Gamma)$  globally and locally, respectively, at Pr=1. Scaling fits (dashed lines) to  $2\pi/\Gamma^*$  over  $Ra \in [10^{10}, 10^{14}]$  and  $2\pi/\Gamma^*_{loc}$  over  $Ra \in [10^{13}, 10^{14}]$  yield exponents of 0.20 and 0.25, respectively. (b) Finite-difference approximations of the local exponent  $\beta_k = d(\log k)/d(\log Ra)$ . The values 1/4 and 1/5 (grey dotted lines) agree with the scaling fit exponents to two digits.

Figure 2(b) shows the Ra-dependent local scaling exponent  $\beta_n = d(\log Nu)/d(\log Ra)$  of the Nu-Ra relation for  $\Gamma = 2$ ,  $\Gamma^*$  and  $\Gamma^*_{loc}$ . This quantity educes small variations not visible in figure 2(a). In particular, for rolls of aspect ratios  $\Gamma^*$ , the exponent  $\beta_n$  exhibits a small but rapid change just below  $Ra = 10^9$ , beyond which it smoothly approaches the classical 1/3 exponent that appears to be the  $Ra \to \infty$  asymptotic behaviour. This rapid change seems to coincide with the velocity becoming vertically uniform outside the boundary layers, as reflected in the streamlines of figure 1(b); further details of the rolls' structure will be reported elsewhere. Rolls with  $\Gamma = 2$  fixed undergo a similarly rapid change around  $Ra \approx 2 \times 10^7$  and then approach  $Nu \sim Ra^{1/4}$  scaling that appears to be asymptotic. Rolls of aspect ratio  $\Gamma_{loc}^*$  show intermediate Nu scaling whose best-fit exponent over the last decade of data is 0.29.

Figure 3(a) shows the Ra-dependence of the wavenumber  $k = 2\pi/\Gamma$  for  $\Gamma^*$  and  $\Gamma_{loc}^*$ compensated by  $Ra^{1/5}$ . The compensated wavenumbers for  $\Gamma^*$  approach a horizontal line, suggesting that the Nu-maximizing rolls narrow according to the power law  $\Gamma^* \sim Ra^{-1/5}$ . This narrowing of  $\Gamma^*$  is slow relative to the case of RBC in a porous medium, where  $\Gamma^* \sim Ra^{-1/2}$  (Wen, Corson & Chini 2015).

Figure 3(b) shows the Ra-dependence of the local scaling exponent  $\beta_k =$  $d(\log k)/d(\log Ra)$ . For  $k=2\pi/\Gamma^*$  the local scaling exponent remains close to 1/5 after the transition around  $Ra=10^9$ . For  $k=2\pi/\Gamma_{loc}^*$  the exponent seems to approach 1/4, suggesting that  $\Gamma_{loc}^*$  has the same  $Ra^{-1/4}$  scaling as the narrowest marginally stable mode. Variations in  $\beta_k$  beyond  $Ra = 10^{12}$  for  $\Gamma^*$  are evident, but these might be due to numerical imprecision: Nu depends very weakly on  $\Gamma$  around the maximum of  $Nu(\Gamma)$ , as seen in figure 1(c), so the value of  $\Gamma^*$  cannot be determined nearly as precisely as the value of  $Nu(\Gamma^*).$ 

## 3.2. Asymptotic kinetic energy

Another emergent quantity central to RBC is the bulk Reynolds number based on root-mean-squared velocity, which in terms of dimensionless solutions

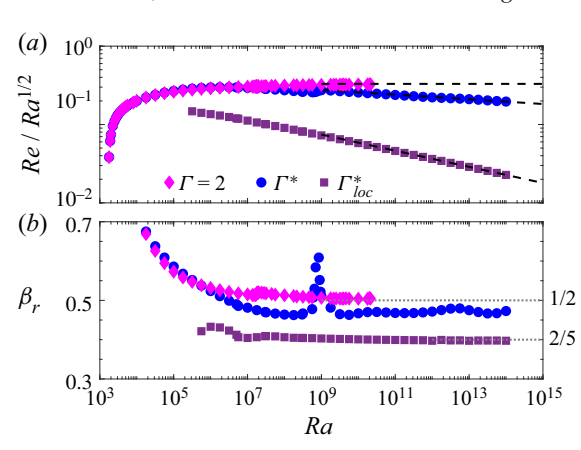


Figure 4. (a) Compensated plot of Re vs Ra for steady rolls with Pr=1 and aspect ratios  $\Gamma=2$ ,  $\Gamma^*$  and  $\Gamma^*_{loc}$ . Scaling fits yield  $Re \sim Ra^{0.50}$  for  $\Gamma=2$  and  $Re \sim Ra^{0.40}$  for  $\Gamma^*_{loc}$  over the last decade of each data set, and  $Re \sim Ra^{0.47}$  for  $\Gamma^*$  over  $Ra \in [10^{10}, 10^{14}]$  (dashed lines). (b) Finite-difference approximations to the local exponent  $\beta_r = d(\log Re)/d(\log Ra)$ . Exponents of 1/2 and 2/5 are shown to guide the eye (grey dotted lines).

to (2.1) is

$$Re = \left(\frac{Ra}{Pr}\right)^{1/2} \langle |\boldsymbol{u}|^2 \rangle^{1/2}.$$
 (3.1)

Figure 4 depicts the dependence of Re on Ra for the steady rolls of aspect ratios  $\Gamma = 2$ ,  $\Gamma^*$  and  $\Gamma_{loc}^*$ . Figure 4(a) shows Re compensated by  $Ra^{1/2}$  while figure 4(b) shows the local scaling exponent  $\beta_r = d(\log Re)/d(\log Ra)$ . Rolls with the fixed aspect ratio  $\Gamma = 2$  approach the asymptotic scaling  $Re \sim Ra^{1/2}$  that corresponds to the root-mean-squared velocity being proportional to the free-fall velocity  $U_f$ . For rolls with Nu-maximizing aspect ratios  $\Gamma^*$ , the scaling fit over  $Ra \in [10^{10}, 10^{14}]$  is  $Re \sim Ra^{0.47}$ , which is quite close to the  $Re \sim Ra^{0.46}$  scaling observed in recent 3-D DNS up to  $Ra = 10^{15}$  at Pr = 1 in a slender cylinder with a height 10 times its diameter (Iyer et al. 2020). For the  $\Gamma_{loc}^*$  rolls, the scaling exponent of Re is indistinguishable from 2/5. The measured exponents (0.50, 0.47, 0.40) are unchanged if Re is defined using the pointwise maximum velocity rather than using the root-mean-squared velocity as in (3.1). All three aspect ratios result in smaller speeds than steady rolls between stress-free boundaries, where  $Re \sim Ra^{2/3}$  for any fixed Pr and  $\Gamma$  (Wen et al. 2020).

#### 4. Comparison with turbulent convection

To compare heat transport by steady rolls with that by turbulent thermal convection, we compiled Nusselt number data from high-Ra DNS with Pr = 1 or 0.7 and laboratory experiments where the estimated Pr is between 0.7 and 1.3. Figure 5 shows these Nu values compensated by  $Ra^{1/3}$ , along with Nu values of steady convection rolls at the Nu-maximizing aspect ratios  $\Gamma^*$ . Strikingly, heat transport by the Nu-maximizing 2-D steady rolls is larger than transport by turbulent convection in all cases.

The turbulent data shown in figure 5, as detailed in the figure caption, include DNS in horizontally periodic 2-D and 3-D domains, wherein 2-D steady rolls solve the equations of motion, as well as 3-D DNS and laboratory experiments in cylinders that do not admit 2-D rolls. Values of Nu for steady rolls with  $\Gamma = 2$  fixed are omitted from figure 5 for clarity, but they lie below all turbulent values once Ra approximately exceeds  $2 \times 10^9$ 

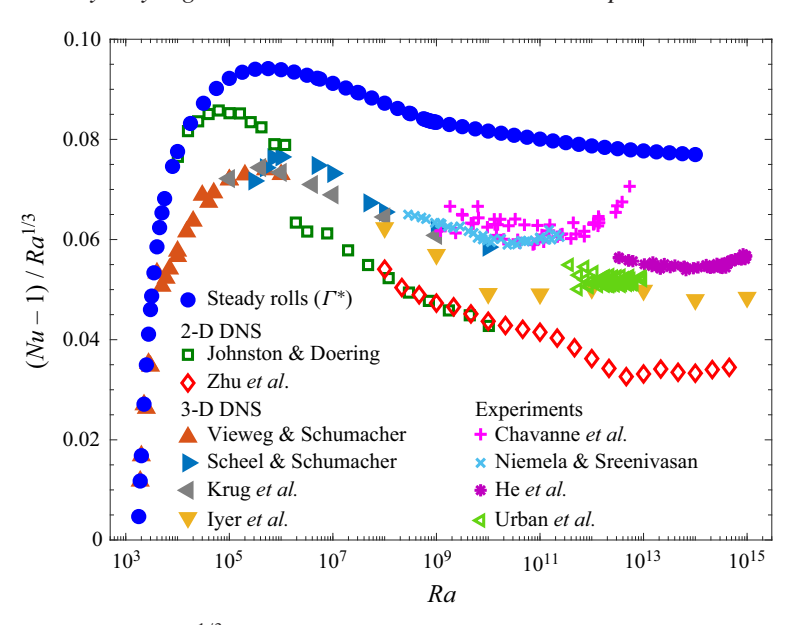


Figure 5. Nu compensated by  $Ra^{1/3}$  for steady rolls of Nu-maximizing aspect ratios  $\Gamma^*$  at Pr = 1, along with Nu from turbulent 2-D and 3-D DNS and experiments with estimated  $Pr \in [0.7, 1.3]$ . For horizontally periodic domains, 2-D DNS with  $(\Gamma, Pr) = (2, 1)$  were done by Johnston & Doering (2009) and Zhu et al. (2018), and 3-D DNS with  $\Gamma \geq 8$  and Pr = 1 were done by Vieweg & Schumacher (personal communication 2020) and Krug, Lohse & Stevens (2020). For DNS in cylinders of diameter-to-height ratio  $\Gamma_c$ , Iyer et al. (2020) used  $(\Gamma_c, Pr) = (0.1, 1)$  and Scheel & Schumacher (2017) used  $(\Gamma_c, Pr) = (1, 0.7)$ . For laboratory experiments in cylinders, where the plotted data are truncated according to  $Pr \in [0.7, 1.3]$ , the domains and estimated Prranges are  $\Gamma_c = 0.5$  and  $Pr \in [0.7, 1.3]$  for Chavanne et al. (2001),  $\Gamma_c = 4$  and  $Pr \in [0.7, 1.27]$  for Niemela & Sreenivasan (2006),  $\Gamma_c = 0.5$  and  $Pr \in [0.79, 0.86]$  for He et al. (2012), and  $\Gamma_c = 1$  and  $Pr \in [0.95, 1.17]$ for Urban et al. (2014). Experiments used working fluids of low-temperature helium gas (Chavanne et al. 2001; Niemela & Sreenivasan 2006; Urban et al. 2014) or sulphur hexafluoride (He et al. 2012).

(cf. figure 2), and this gap would only widen at larger Ra if their  $Nu \sim Ra^{1/4}$  scaling persists. The laboratory data sets in figure 5 have unavoidably varying Pr values that can be hard to estimate, as well as non-Oberbeck-Boussinesq effects (Urban, Musilová & Skrbek 2011; Urban et al. 2012, 2014). The figure includes only a narrow range of estimated Pr values in order to avoid significant non-Oberbeck-Boussinesq effects. When data over a wider range of estimated Pr is included, a few data points from the experiments of Chavanne et al. (2001) lie above the  $Nu(\Gamma^*)$  values of steady rolls, as shown in the supplementary material.

Our finding that steady rolls of Nu-maximizing aspect ratios apparently display classical  $Nu \sim Ra^{1/3}$  asymptotic scaling does not ineluctably imply anything about turbulent convection. Taking a dynamical systems point of view, however, steady solutions admitted by the domain are fixed points of (2.1), so they and their unstable manifolds are part of the global attractor. Turbulent trajectories may linger near these fixed points and so inherit some quantitative features (Kooloth et al. 2021), as has been found for unstable coherent states in shear flows (Nagata 1990; Waleffe 1998; Wedin & Kerswell 2004; Gibson, Halcrow & Cvitanović 2008; Suri et al. 2020; Graham & Floryan 2021). Indeed, figure 5 shows scaling similarities between steady and turbulent convection. Further exploration of the global attractor calls for study of 3-D steady flows. Recently computed 'multi-scale' 3-D steady states (Motoki et al. 2021) give larger Nu values than all 2-D rolls

### B. Wen, D. Goluskin and C.R. Doering

at moderate Ra, but their scaling at large Ra is unknown. Simpler 3-D steady convection patterns remain to be computed as well. Analytically, it is an open challenge to construct approximations of 2-D or 3-D steady flows that are asymptotically accurate as  $Ra \to \infty$ , as has been done for 2-D rolls between stress-free boundaries (Chini & Cox 2009; Wen et al. 2020). Such constructions could be used to verify that  $Nu \sim Ra^{1/3}$  is indeed the exact asymptotic scaling for the Nu-maximizing rolls we have computed, as well as to determine the precise Re-Ra scaling relations for rolls of both Nu- and Re-maximizing aspect ratios.

More generally, figure 5 highlights the absence of reproducible evidence for ultimate  $Nu \sim Ra^{1/2}$  scaling, and it raises the intriguing possibility that steady rolls with  $Nu \sim Ra^{1/3}$  might transport more heat than turbulent convection as  $Ra \to \infty$ . We know of no counterexamples to this hypothesis, including in the case of stress-free boundaries (Wen et al. 2020). Heat transport by solutions of (2.1) with no-slip isothermal boundaries has been mathematically proved to be limited by  $Nu \le O(Ra^{1/2})$  (Howard 1963; Doering & Constantin 1996), but it remains unknown whether any solutions attain the ultimate scaling of this upper bound. One avenue for pursuing a stronger mathematical statement is to study two conjectures suggested by our computations: that steady convection maximizes Nu among all solutions of (2.1) regardless of their stability or time-dependence, and that steady solutions of (2.1) are subject to an upper bound of the form  $Nu \leq O(Ra^{1/3})$ . Therefore, although numerically computed flows can never determine  $Ra \to \infty$  scaling definitively, our results suggest a new mathematical approach that may be able to finally resolve the question of asymptotic Nu scaling in turbulent convection.

Supplementary material. Supplementary material is available at https://doi.org/10.1017/jfm.2021.1042.

Acknowledgements. After this manuscript was written our senior author, C.R. Doering, passed away too soon. Beyond his many contributions to the present study, we are forever indebted to him for his mentorship, to say nothing of his many lasting contributions to the field of fluid dynamics. He will be deeply missed by us and many others. We also want to acknowledge helpful discussions about the present work with L.M. Smith, D. Sondak and F. Waleffe.

This work was supported by US National Science Foundation awards (DMS-1515161, DMS-1813003), Canadian NSERC Discovery Grants Program awards (RGPIN-2018-04263, RGPAS-2018-522657, DGECR-2018-00371) and computational resources provided by Advanced Research Computing at the University of Michigan.

**Declaration of interests.** The authors report no conflict of interest.

#### Author ORCIDs.

- Baole Wen https://orcid.org/0000-0003-2073-1508;
- David Goluskin https://orcid.org/0000-0003-3109-0830;
- Charles R. Doering https://orcid.org/0000-0003-2769-8026.

#### REFERENCES

CHAVANNE, X., CHILLA, F., CHABAUD, B., CASTAING, B. & HEBRAL, B. 2001 Turbulent Rayleigh-Bénard convection in gaseous and liquid He. Phys. Fluids 13, 1300-1320.

CHILLÀ, F. & SCHUMACHER, J. 2012 New perspectives in turbulent Rayleigh-Bénard convection. Eur. Phys.

CHINI, G.P. & COX, S.M. 2009 Large Rayleigh number thermal convection: heat flux predictions and strongly nonlinear solutions. Phys. Fluids 21, 083603.

DOERING, C.R. 2020 Turning up the heat in turbulent thermal convection. Proc. Natl Acad. Sci. USA **117**, 9671–9673.

DOERING, C.R. & CONSTANTIN, P. 1996 Variational bounds on energy dissipation in incompressible flows. III. Convection. Phys. Rev. E 53, 5957-5981.

- DOERING, C.R., OTTO, F. & REZNIKOFF, M.G. 2006 Bounds on vertical heat transport for infinite-Prandtl-number Rayleigh-Bénard convection. J. Fluid Mech. 560, 229-241.
- GIBSON, J.F., HALCROW, J. & CVITANOVIĆ, P. 2008 Visualizing the geometry of state space in plane Couette flow. J. Fluid Mech. 611, 107-130.
- GRAHAM, M.D. & FLORYAN, D. 2021 Exact coherent states and the nonlinear dynamics of wall-bounded turbulent flows. Annu. Rev. Fluid Mech. 53, 227-253.
- HE, X., FUNFSCHILLING, D., NOBACH, H., BODENSCHATZ, E. & AHLERS, G. 2012 Transition to the ultimate state of turbulent Rayleigh-Bénard convection. Phys. Rev. Lett. 108, 024502.
- HOWARD, L.N. 1963 Heat transport by turbulent convection. J. Fluid Mech. 17, 405-432.
- IYER, K.P., SCHEEL, J.D., SCHUMACHER, J. & SREENIVASAN, K.R. 2020 Classical 1/3 scaling of convection holds up to  $Ra = 10^{15}$ . Proc. Natl Acad. Sci. USA 117, 7594–7598.
- JEFFREYS, H. 1928 Some cases of instability in fluid motion. Proc. R. Soc. A 118, 195-208.
- JOHNSTON, H. & DOERING, C.R. 2009 Comparison of turbulent thermal convection between conditions of constant temperature and constant flux. Phys. Rev. Lett. 102, 064501.
- KADANOFF, L.P. 2001 Turbulent heat flow: structures and scaling. *Phys. Today* **54**, 34–39.
- KOOLOTH, P., SONDAK, D. & SMITH, L.M. 2021 Coherent solutions and transition to turbulence in two-dimensional Rayleigh–Bénard convection. *Phys. Rev. Fluids* **6**, 013501.
- KRUG, D., LOHSE, D. & STEVENS, R.J.A.M. 2020 Coherence of temperature and velocity superstructures in turbulent Rayleigh–Bénard flow. J. Fluid Mech. 887, A2.
- MOTOKI, S., KAWAHARA, G. & SHIMIZU, M. 2021 Multi-scale steady solution for Rayleigh-Bénard convection. J. Fluid Mech. 914, A14.
- NAGATA, M. 1990 Three-dimensional finite-amplitude solutions in plane Couette flow: bifurcation from infinity. J. Fluid Mech. 217, 519-527.
- NIEMELA, J.J. & SREENIVASAN, K.R. 2006 Turbulent convection at high Rayleigh numbers and aspect ratio 4. J. Fluid Mech. 557, 411–422.
- OLSON, M.L., GOLUSKIN, D., SCHULTZ, W.W. & DOERING, C.R. 2021 Heat transport bounds for a truncated model of Rayleigh-Bénard convection via polynomial optimization. *Physica D* 415, 132748.
- OTTO, F. & SEIS, C. 2011 Rayleigh-Bénard convection: improved bounds on the Nusselt number. J. Math. Phys. 52, 083702.
- RAYLEIGH, LORD 1916 On convection currents in a horizontal layer of fluid, when the higher temperature is on the under side. Phil. Mag. 32, 529-546.
- SCHEEL, J.D. & SCHUMACHER, J. 2017 Predicting transition ranges to fully turbulent viscous boundary layers in low Prandtl number convection flows. Phys. Rev. Fluids 2, 123501.
- SONDAK, D., SMITH, L.M. & WALEFFE, F. 2015 Optimal heat transport solutions for Rayleigh-Bénard convection. J. Fluid Mech. 784, 565-595.
- SURI, B., KAGEORGE, L., GRIGORIEV, R.O. & SCHATZ, M.F. 2020 Capturing turbulent dynamics and statistics in experiments with unstable periodic orbits. Phys. Rev. Lett. 125, 064501.
- TREFETHEN, L.N. 2000 Spectral Methods in MATLAB. SIAM.
- Urban, P., Hanzelka, P., Kralik, T., Musilova, V., Srnka, A. & Skrbek, L. 2012 Effect of boundary layers asymmetry on heat transfer efficiency in turbulent Rayleigh-Bénard convection at very high Rayleigh numbers. Phys. Rev. Lett. 109, 154301.
- Urban, P., Hanzelka, P., Musilová, V., Králík, T., La Mantia, M., Srnka, A. & Skrbek, L. 2014 Heat transfer in cryogenic helium gas by turbulent Rayleigh-Bénard convection in a cylindrical cell of aspect ratio 1. New J. Phys. 16, 053042.
- URBAN, P., MUSILOVÁ, V. & SKRBEK, L. 2011 Efficiency of heat transfer in turbulent Rayleigh-Bénard convection. Phys. Rev. Lett. 107, 014302.
- WALEFFE, F. 1998 Three-dimensional coherent states in plane shear flows. *Phys. Rev. Lett.* 81, 4140.
- WALEFFE, F., BOONKASAME, A. & SMITH, L.M. 2015 Heat transport by coherent Rayleigh-Bénard convection. Phys. Fluids 27, 051702.
- WEDIN, H. & KERSWELL, R.R. 2004 Exact coherent structures in pipe flow: travelling wave solutions. J. Fluid Mech. 508, 333-371.
- WEN, B. & CHINI, G.P. 2018 Inclined porous medium convection at large Rayleigh number. J. Fluid Mech. **837**, 670–702.
- WEN, B., CORSON, L.T. & CHINI, G.P. 2015 Structure and stability of steady porous medium convection at large Rayleigh number. J. Fluid Mech. 772, 197–224.
- WEN, B., GOLUSKIN, D., LEDUC, M., CHINI, G.P. & DOERING, C.R. 2020 Steady coherent convection between stress-free boundaries. J. Fluid Mech. 905, R4.
- WHITEHEAD, J.P. & DOERING, C.R. 2011 Ultimate state of two-dimensional Rayleigh–Bénard convection between free-slip fixed-temperature boundaries. *Phys. Rev. Lett.* **106**, 244501.

## B. Wen, D. Goluskin and C.R. Doering

WHITEHEAD, J.P. & DOERING, C.R. 2012 Rigid bounds on heat transport by a fluid between slippery boundaries. *J. Fluid Mech.* **707**, 241–259.

ZHU, X., MATHAI, V., STEVENS, R.J.A.M., VERZICCO, R. & LOHSE, D. 2018 Transition to the ultimate regime in two-dimensional Rayleigh–Bénard convection. *Phys. Rev. Lett.* **120**, 144502.